Controlled Kinetic Monte Carlo Simulation for Computer-Aided Nanomanufacturing

Yan Wang
Woodruff School of Mechanical Engineering,
Georgia Institute of Technology,
Atlanta, GA 30332
e-mail: yan.wang@me.gatech.edu

Kinetic Monte Carlo (KMC) is regarded as an efficient tool for rare event simulation and has been applied in simulating bottom–up self-assembly processes of nanomanufacturing. Yet it has limitations to simulate top–down processes. In this paper, a new and generalized KMC mechanism, called controlled KMC or controlled KMC (cKMC), is proposed to simulate complete physical and chemical processes. This generalization is enabled by the introduction of controlled events. In contrast to the traditional self-assembly events in KMC, controlled events occur at certain times, locations, or directions, which allows all events to be modeled. A formal model of cKMC is also presented to show the generalization. The applications of cKMC to several top–down and bottom–up processes are demonstrated. [DOI: 10.1115/1.4031461]

1 Introduction

In product and process design, computational tools allow engineers to predict behaviors of products and performance of manufacturing processes. Similar to computer-aided manufacturing (CAM) tools that have been applied in traditional manufacturing to reduce the cost and improve the quality of products, computer-aided nanomanufacturing (CANM) tools are valuable to design the process of nanomanufacturing. Computing and information technologies will play a significant role in the success of new nanomanufacturing systems. Effectiveness and efficiency must be considered early in the design cycle for maximum impact [1]. The repeatability and scalability of nanomanufacturing processes are the major challenges for the application of nanotechnology. Compared to experimental study, simulation is a cost-effective way to understand the complex physical and chemical processes at nanoscales. It can help predict and correct potential manufacturing problems at early stages, thus eliminating otherwise induced wastes and costs. Simulation-based process planning and optimization in CANM thus are very necessary for the advancement of nanomanufacturing.

In general, nanomanufacturing techniques are classified as either top–down or bottom–up [2–4]. In the top–down approaches, materials are removed with low volumes and sizes down to the scale of dozens of nanometers. In the bottom–up approaches, materials are assembled under the guidance of nanoscale templates, either physically or chemically. Simulation is the core methodology of CANM. Molecular dynamics (MD) simulation has been used to study top–down atomic scale machining in the past two decades [5]. MD was used to simulate nano-lithography [6,7] and cutting with diamond tools [8–11]. For other processes, MD has been used to simulate nanoindentation [12], laser ablation of bulk materials [13], and laser-based sintering [14]. However, the major issue of MD is its short-time scale, which is not compatible with those in nanomanufacturing. MD simulates behaviors at the time scales ranging from femto to nanoseconds. Most of the computational time in MD is spent on the thermal vibration of atoms, instead of our interested processes that are usually longer than microseconds. Those events of interest with longer time scale than thermal vibration are rare events. MD simulation is very inefficient in simulating these rare events. Unrealistic assumptions have to be made to accommodate the time scale. For instance, extremely high cutting speed (e.g., 100 m/s) was used in the preceding MD simulation studies, which only simulate picoseconds of the processes. With such speed and time scale, the accuracy of predictions on required forces, defects, and others is affected.

To simulate the rare events of transitions or reactions, several improvements of MD have been proposed to bridge the gap of time scale and accelerate the simulation speed of rare events, such as by running multiple trajectories [15], introducing bias potentials [16], or increasing temperatures [17]. However, the inherent inefficiency of MD is that computational time is spent on trajectory prediction, which is not important for rare event simulations. Compared to MD, atomic scale KMC [18] is more efficient in simulating the infrequent transition processes with times longer than thermal vibrations.

In KMC, various discrete *events* or *processes* are defined. During simulation, the discrete events are generated and fired sequentially based on their respective probabilities of occurrence, which are usually assumed to be exponential distributions. This assumption is necessary to make KMC mathematically sound and theoretically tractable. These probabilities can be calculated from the reaction or transition rate constants, which could be estimated from either experiments or first-principles calculations.

KMC has been widely used to simulate chemical reactions and some of the bottom–up self-assembly processes such as chemical vapor deposition (CVD) and physical vapor deposition (PVD). Yet it has not been considered to simulate general nanomanufacturing processes, particularly those top–down processes. In this paper, a novel and generic KMC simulation mechanism is proposed to simulate nanomanufacturing processes. The new mechanism is called controlled kinetic Monte Carlo (cKMC). The goal is to provide an efficient and unified simulation framework for CANM to enable both top–down and bottom–up nanomanufacturing processes.

For the rest of the paper, the background of KMC is first given in Sec. 2. In Sec. 3, the cKMC simulation framework is proposed and illustrated by several top–down and bottom–up processes. The implementation details are described in Sec. 4.

2 Background

KMC is a useful tool to simulate systems at multiple time scales with rare events. In this section, the introductions of KMC and its application in some bottom–up self-assembly processes are given.

Contributed by the Manufacturing Engineering Division of ASME for publication in the JOURNAL OF MICRO- AND NANO-MANUFACTURING. Manuscript received March 21, 2014; final manuscript received August 22, 2015; published online September 23, 2015. Assoc. Editor: John P. Coulter.

2.1 KMC Simulation. In KMC, various discrete events (also called *processes*) are defined. For instance, in the CVD process of crystal growth, the major types of events include: *adsorption* (particles in vapor are attracted to the solid surface), *desorption* (particles previously absorbed on the solid surface escape and are vaporized), *diffusion* (particles on the surface or in the solid move to a different location), and *surface reaction* (gas precursors react and generate solid products).

During KMC simulation, discrete events are generated and fired sequentially based on their respective probabilities of occurrence, which are exponential distributions in general. The transition rate (also called propensity function) a_j from current state to state j is $a_j = \nu_j \exp(-\Delta E_j/k_B T)$, where k_B is the Boltzmann constant, T is the temperature, ΔE_j is the energy barrier between the current state and state j, and ν_j is the pre-exponential factor that can be measured or calculated from the vibrational frequencies, e.g., based on the harmonic transition state theory [19,20].

Among all M possible events leaving current state, the probability p_j for event j is $p_j = a_j/a_0$ where $a_0 = \sum_{i=1}^{M} a_i$. Because the time between two transition events of type j, T_j, is exponentially distributed as $T_j \sim \text{exponential}(a_j)$, and the probability that the inter-arrival time of event j is the minimum among M independent events is $P[T_j = \min(T_1, \ldots, T_M)] = a_j/a_0$. Therefore random event selection is based on the uniform sampling with the selection ratio of a_j/a_0. Once event j is fired with the probability p_j, the time of the system is advanced by another random value $\Delta t \sim \text{exponential}(a_0)$, which is the earliest occurring time for any one out of the M independent events that are exponentially distributed. That is, the clock advances by $\Delta t = -\ln(u)/a_0$ where $u \sim U(0,1)$ is a random number uniformly distributed between 0 and 1. Notice that the propensity functions a_j 's (thus the total propensity a_0) and the number of available events M are time-dependent. This event selection and clock advancement algorithm is the most used one and often referred as the direct method [21]. In addition, new data structures and algorithms have been developed to improve the efficiency in searching the events [22–24].

KMC is an effective solution for rare event simulation. Yet it faces three major technical challenges. First, ideally all events have to be known a priori and listed in the event catalog so that the dynamics of physical process can be simulated accurately. Second, during simulation, the occurring probabilities of events are assumed to be accurate and fixed. Third, the time scales of the events may vary significantly; thus computational time is not optimized to focus more on slower but critical events. Recently, some solutions were proposed to resolve some of the preceding issues. The current paper will not address these issues (see Ref. [25] for more information).

2.2 KMC Simulation of Self-Assembly Processes. In the domain of nanomanufacturing, KMC simulation has been used in some of the bottom–up processes. For PVD, it is used to simulate deposition and diffusion events in sputtering (e.g., Refs. [26,27]). The additional research question is how to incorporate extra information of kinetic energy in particles to make correct predictions, such as reflection, resputtering, latent heat, kinetic energy induced diffusion, and others [28–30]. Approximations based on MD and the embedded atom method are applied. For CVD processes, KMC is used to simulate onsite chemical reaction events of film growth (e.g., Refs. [31–34]) and etching (e.g., Refs. [35–37]).

The major issue in KMC simulation of bottom–up self-assembly processes is the accuracy of reaction or transition rates used in simulation because not much experimental data are available. Alternatively, the rates can be estimated by first-principles simulation. Efforts to integrate density functional theory and KMC have been taken to simulate CVD processes of diamond growth [38], molecular beam epitaxial growth of compound semiconductors [39], catalytic decomposition and surface reaction [40], and others.

KMC simulation has not been applied in top–down processes. The main reason is that the traditional KMC has no direct control on *where* and *when* an event takes place. They are stochastically determined by random sampling. In top–down processes, stochastic events are mixed with deterministic ones, where precise locations of manipulation are controllable. In this paper, a generalized KMC mechanism, called controlled KMC, is proposed to simulate both bottom–up and top–down processes.

3 The Proposed Controlled KMC Simulation

In the bottom–up processes, the simulated events mainly include thermally or chemically induced atomic rearrangements such as diffusion, absorption, desorption, surface reaction, and abstraction. These rearrangements occur spontaneously in the form of self-assembly. Those spontaneous events are called *self-assembly events*. In the top–down processes, the atomic rearrangement is triggered by some external energy sources such as force or electromagnetic field. The rearrangement is further induced by self-assembly events. These external events could be scanning probe tip interaction with samples, bombardment of high-energy particles, molding materials with attractive and repulsive forces, and others. These external events are scheduled to occur at certain locations, toward certain directions, or at particular times to control the overall process. Therefore they are called *controlled events*. The major new concept in cKMC is the introduction of controlled events in the algorithm to simulate top–down processes in parallel with bottom–up processes.

The main parameters for both self-assembly and controlled events are how often the events occur, specified as rates. Additional parameters are introduced for controlled events, including when and where the events may occur. When controlled events occur could be deterministic. For example, in atomic force microscopy (AFM) nanolithography, the time when the cutting tip reaches one particular position along the predetermined path is fixed. Furthermore, the spatial location where a controlled event occurs could also be predetermined. For example, in kinetic energy induced diffusion (e.g., focused ion beam (FIB) and electron beam (e-beam) lithography under electromagnetic field), the preferred directions that particles move toward are fixed. Therefore in the cKMC simulation, there is a time, a direction vector, or both associated with a controlled event. As the simulation clock is advanced based on self-assembly events, controlled events are checked constantly so that those with the predetermined time earlier than the current time should be fired. If a predetermined direction is associated with a controlled event and the reaction or transition direction is different, then the event is aborted (more details will be described in the remainder of Sec. 3).

Notice that the particles in the KMC are not necessarily atoms only. They could be electrons, photons, monomers, or molecules as long as the inside structure and behavior are not of interest and assumed to be at an equilibrium state. It also should be noted that controlled events are not only necessary to simulate top–down processes but also useful for some bottom–up processes such as controlled growth of carbon nanotube with directed orientations, which so far still largely depends on MD simulation.

3.1 An Illustration With Scanning Probe Lithography. Here the scanning probe lithography process is used to illustrate the basic idea of cKMC. For the model in Fig. 1, besides the regular *workpiece species*, there is a *controlled species*, even though chemically they could be identical. Controlled species are species where the times of associated events are deterministic. That is, the events will be fired at prescheduled times. In this case, it is based on the moving speed of the probe. The locations of controlled species are also predetermined based on the planned scanning or cutting path. There is also a *vaporized workpiece species,* which escapes the solid body of workpiece in regular diffusion. In the

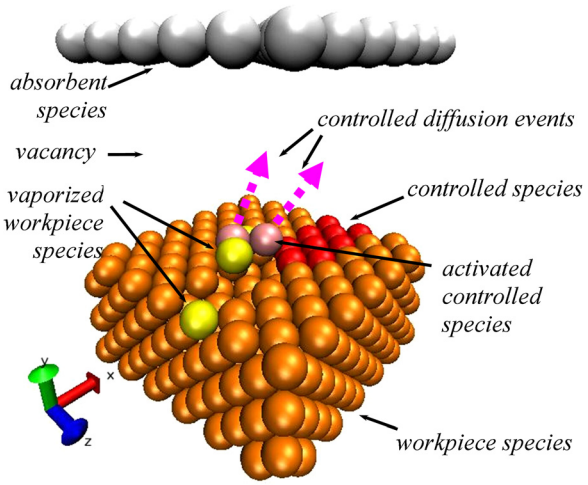

Fig. 1 Illustration of scanning probe lithography events

controlled reaction of the controlled species, atoms of the controlled species are converted to *activated control species* based on the scheduled times sequentially. Here the probe is moving along the path denoted by the sites of controlled species along the *x*-axis direction from left to right. The atoms of controlled species on the left have earlier time of conversion than those on the right. The activated control species has a higher kinetic energy than the vaporized workpiece species. Therefore they are associated with *controlled diffusion events*. The controlled diffusion events have several restrictions, such as the *controlled directions* (illustrated by the dotted arrows in Fig. 1) by which activated atoms can diffuse to neighboring sites or by which they can interact with neighboring atoms of workpiece species. In addition, vacancy exists between occupied spatial lattices. Therefore a *vacancy species* can be defined. Finally, there is an *absorbent species* at the boundary of simulated domain, where the lifecycle of the atoms of vaporized workpiece species and controlled species are terminated.

In the simplified scanning probe lithography process in Fig. 1, several example events are listed in Table 1. Events are organized into several categories based on the number of neighboring sites involved. Events are denoted by reaction-like equations. The left of the equations are reactants and the right are products. The first reactant is the owner of the event, meaning that the event is associated with the site where the first reactant initially resides. After the reaction, the reactant species are replaced by the product species at the corresponding sites. Among the events in Table 1, reaction R1 has only one site involved. It is a controlled event when the controlled species is converted to the activated controlled species based on the scheduled time along the cutting path. R2–R6 have two neighboring sites involved. R2 is the controlled diffusion event associated with activated controlled species. It models the effect of kinetic energy associated with particles transferred from the moving probe. A particle of activated controlled species can diffuse to a vacant neighboring site if the direction from the current site to the vacant site is aligned with the controlled direction. In contrast, R3 and R4 are regular diffusion events without directional constraints. R5 and R6 absorb particles at the boundary of simulation. When vaporized workpiece species and activated control species approach absorbent species at the boundary of simulation domain, they are removed from the domain and the corresponding sites become vacant. Among the reactions with three reactants, R7 is a coordinated diffusion event where three sites are involved. It has been revealed by first-principles simulation that coordinated diffusion with multiple sites involved could have lower energy barriers than the traditional single-hop diffusion (e.g., in R4) as originally thought [41,42]. R8 is an adsorption event. When an atom of vaporized workpiece species is surrounded by two atoms of workpiece species, it has a chance to be attached to the solid surface. For reactions with four reactants, R9 is an example interaction between the activated controlled species and the workpiece species where kinetic energy is transferred. R10 is another absorption event when an atom of vaporized workpiece species is surrounded by three atoms of workpiece species. The kinetic energy of the atom is absorbed, and it settles down onto the solid surface. It should be noted that Table 1 only lists some examples. More events can be introduced in a similar format, which allows for necessary refinement and extension.

The controlled events can be generally used in various complex top–down fabrication processes. In MD simulation, special treatments of potential energy between atoms of workpiece and tool are needed so that the rapid movement of atoms can be modeled. Here controlled events are used to model the special movement of atoms under directional constraints.

3.2 Detailed cKMC Algorithm. The key components of the cKMC are the controlled species and controlled events. Controlled species can be specified by an input script ***control_species*** *reactant rate product x y z neighbor_lower neighbor_upper init_time* where ***control_species*** is the command, *reactant* is the name of controlled species, *product* is the resultant species in the controlled reaction, *rate* is the numerical value of reaction rate, and *x*, *y* and *z* specify the direction along which the reaction occur. That is, the reactants of controlled species react and convert to products

Table 1 Example events in scanning probe lithography

Number of sites involved	Reaction/transition event
1	R1: controlled_species → activated_controlled_species (controlled)
2	R2: activated_controlled_species + vacancy → vacancy + activated_controlled_species (controlled) R3: vaporized_workpiece_species + vacancy → vacancy + vaporized_workpiece_species R4: workpiece_species + vacancy → vacancy + workpiece_species R5: vaporized_workpiece_species + absorbent → vacancy + absorbent R6: activated_controlled_species + absorbent → vacancy + absorbent
3	R7: workpiece_species + workpiece_species + vacancy → vacancy + workpiece_species + workpiece_species R8: vaporized_workpiece_species + workpiece_species + workpiece_species → workpiece_species + workpiece_species + workpiece_species
4	R9: activated_controlled_species + workpiece_species + vacancy + vacancy → vacancy + workpiece_species + vacancy + vaporized_workpiece_species R10: activated_controlled_species + workpiece_species + workpiece_species + workpiece_species → workpiece_species + workpiece_species + workpiece_species + workpiece_species

Table 2 Pseudocode of the cKMC algorithm

Initiate regular lattice sites;
Specify regular species on each regular site;
FOR $i = 1$: *numControlSpecies*
    generate the list $controlSpeciesSites_i$ for the ith controlled species;
    calculate *keyvalue* of the ith controlled species;
    sort $controlSpeciesSites_i$ based on *keyvalue*;
END
Define all possible events;
Specify controlled events;
WHILE stop criteria are not met
    Update a list of J active sites with $sitePropensity_j > 0$ for site j
    where $sitePropensity_j = \sum_k propensity_{jk}$ is sum of all event propensities at site j
    Update $totalProp = \sum_{j=1}^{J} sitePropensity_j$;
    //choose a site for the next event
    Generate $r_1 \sim Uniform(0, 1)$;
    Find mth site where $\sum_{j=1}^{m-1} sitePropensity_j < totalProp \times r_1 \leq \sum_{j=1}^{m} sitePropensity_j$;
    //choose an event from the chosen site
    Generate $r_2 \sim Uniform(0, 1)$;
    Find nth event where $\sum_{k=1}^{n-1} propensity_{mk} < sitePropensity_m \times r_2 \leq \sum_{k=1}^{n} propensity_{mk}$;
    Fire event n at site m and update species at neighboring sites;
    //update event list
    FOR all events associated with site m that are not controlled
      OR events are controlled AND controlled event criteria are met
        Add the event into the event list of site m;
    END
    Update propensities for site m and neighboring sites;
    //update system time
    Generate $r_3 \sim Uniform(0, 1)$;
    Advance system time T to $T + \Delta t$ where $\Delta t = -\ln r_3 / totalProp$;
    //update the status of controlled species sites
    FOR $i = 1 : numControlSpecies$
        Fire all controlled events in $controlSpeciesSites_i$ with $keyvalue < T$;
    END
END

sequentially along the specified direction at the rate. The next two integer values, *neighbor_lower* and *neighbor_upper* specify the lower and upper bounds of neighboring sites where the controlled species may react. If the number of its neighbors is not within the bound, the controlled reaction is not initiated. This provides more controls on where controlled reactions can occur. Finally *init_time* specifies when the controlled reaction is started.

Similarly events can be specified by the input script ***event*** *reactant_1* (*reactant_2*, etc.) *rate product_1* (*product_2*, etc.) where ***event*** is the command, *rate* is the numerical value of reaction rate, and corresponding reactants and products at the particular site are defined. For instance, after the event is fired, reactant_1 is replaced by product_1, reactant_2 by product_2, and so on.

Controlled events are specified in two types. The first type is by the direction along which the reaction is going toward, and the second one is by the target location where the reaction is targeted at. The input script is ***control_event*** *index dx dy dz* x_0 y_0 z_0 *theta neighbor_lower neighbor_upper*" where ***control_event*** is the command, *index* refers to the event index previously specified by the command *event*, *dx*, *dy* and *dz* specify the direction which the first and second reactants should be aligned with, and *theta* is an angular allowance such that the direction formed by the first and second reactants can be within the range of $\pm$ *theta* and the reaction still occurs. In other words, the controlled events provide directional selections of events. Controlled events are only fired if the direction formed by the first two reactants is the specified direction or close enough within the $\pm$ *theta* range. Before a controlled event is inserted into the event list, the directional criterion is checked. Those controlled events that do not satisfy the constraints are disregarded. When $dx = dy = dz = 0$, x_0, y_0, and z_0 take effect, and they specify the target location by which the direction of reaction is from the current site to the target location. Two cases can be specified. When *theta* is positive, the reaction direction "converges" toward the target location. When *theta* is negative, the reaction direction "diverges" away from the target location. Similarly, if the direction formed by the first two reactants is far from the specified, events are discarded. Again, *neighbor_lower* and *neighbor_upper* specify the lower and upper bounds of neighboring sites where the controlled event may occur. Therefore rather than directly modeling kinetic energy, controlled events provide a directional selection for cKMC.

Before a simulation starts, all species, sites, and events are specified by script commands. Internally species, controlled species, events, controlled events, reaction sites, and others are stored in array-type data structures. For each site where a controlled species resides, there is an associated *key value*, which usually is the time when the controlled reaction occurs at site j of controlled species i, which is calculated as $t_{ij} = t_i^0 + (\mathbf{r}_{ij} \cdot \mathbf{s}_i - d_i)/a_i$

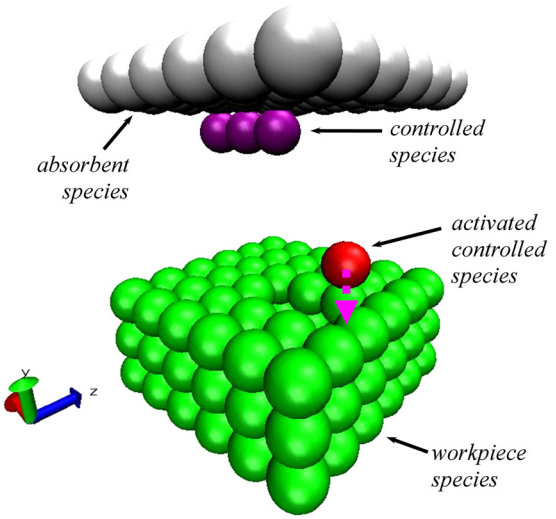

Fig. 2 Illustration of FIB events

where t_i^0 is the reaction start time for controlled species i as previously specified by *init_time*, $\mathbf{r}_{ij}$ is the three-dimensional coordinate of site j of ith controlled species, $\mathbf{s}_i$ is the direction of controlled reaction for controlled species i, d_i is calculated as $d_i = \min_j(\mathbf{r}_{ij} \cdot \mathbf{s}_i)$, and a_i is the reaction rate for controlled species i. In this way, the sites of controlled species are sorted based on the keyvalues corresponding to the reaction direction so that the controlled reactions can be fired deterministically and the time is controllable. Nevertheless, keyvalues can be values other than times if necessary. Table 2 lists the pseudocode of the cKMC algorithm.

3.3 The Formal Model of cKMC. In this section, a formal model of cKMC is provided as a rigorous proof that cKMC is a generalization of the conventional KMC. Suppose that a system consisting of N state variables that form the state vector $\mathbf{X}(t) = (X_1(t), \ldots, X_N(t)) \in \mathbb{Z}_+^N$ at time t where $\mathbb{Z}_+ = \mathbb{N} \cup \{0\}$ is the set of non-negative integers. There are a total of M events or reaction channels R_j's $(j = 1, \ldots, M)$, each of which is characterized by a propensity function $a_j(\mathbf{X}(t) = \mathbf{x})$ or $a_j(\mathbf{x})$ given the current state $\mathbf{x}$, where $a_j : \mathbb{Z}_+^N \to \mathbb{R}_+$, and its state change vector $\mathbf{v}_j = (v_{j1}, \ldots, v_{jN})$. $a_j(\mathbf{X}(t))$ indicates how likely event R_j will be fired in the next infinitesimal time interval and transit out of the current state, defined as $p(\mathbf{X}(t+\delta)|\mathbf{X}(t)) = a_j(\mathbf{X}(t))\delta + o(\delta)$ where $\lim_{\delta \to 0} o(\delta)/\delta = 0$, and $o(0) = 0$. From the sum of propensity function $a_0(\mathbf{X}(t)) = \sum_{j=1}^M a_j(\mathbf{X}(t))$, the probability of firing R_j at time t is $P(R_j, t) = a_j(\mathbf{X}(t))/a_0(\mathbf{X}(t))$.

The theoretical model of KMC, the *chemical master equation*, states that

$$\frac{d}{dt}p(\mathbf{X}(t) = \mathbf{x}|\mathbf{X}(t_0) = \mathbf{x}_0) = \sum_{j=1}^{M} a_j(\mathbf{x} - \mathbf{v}_j)p(\mathbf{X}(t) = \mathbf{x} - \mathbf{v}_j|\mathbf{X}(t_0) = \mathbf{x}_0) - \left[\sum_{j=1}^{M} a_j(\mathbf{x})p(\mathbf{X}(t) = \mathbf{x}|\mathbf{X}(t_0) = \mathbf{x}_0)\right] \quad (1)$$

where $p(\mathbf{X}(t) = \mathbf{x}|\mathbf{X}(t_0) = \mathbf{x}_0)$ is the probability of $\mathbf{X}(t) = \mathbf{x}$ given the initial distribution $\mathbf{X}(t_0) = \mathbf{x}_0$. Equation (1) describes the evolution of the probability distribution of the system, which has the Markov property. It also models a continuous-time Markov chain.

For a particular set of states $\{\mathbf{x}_d\}$ and times $\{t_k\}$ for which controlled events R_C's are defined, $a_C(\mathbf{x}_d, t_k) = \delta(t - t_k)$ where $\delta(t)$ is the Dirac delta function. That is, when a prescheduled deterministic event occurs, the corresponding rate for R_C is $a_C(\mathbf{x}_d, t_k) = \infty$. Therefore the probability that R_C is fired is one. Equation (1) generally describes the evolution of the probability distribution of the system modeled by cKMC. When $\{\mathbf{x}_d\} = \varnothing$ and $\{t_k\} = \varnothing$, cKMC just becomes the classical KMC.

3.4 More Examples of cKMC With Controlled Events

3.4.1 FIB. In FIB, high-energy particles such as ions or electrons are projected to workpieces to modify structures locally via physical or chemical interactions. The obvious advantage of KMC approaches is that chemical reactions can be simulated easily. The proposed cKMC can simultaneously simulate the controlled physical interactions and chemical reactions. Therefore more complex processes such as FIB assisted chemical vapor deposition can be simulated in the same way.

As illustrated in Fig. 2, the controlled species is the source of ions (e.g., gallium and gold/silicon alloy) or electron beams. They are selectively allocated to some lattice locations based on the specified milling path. When the controlled species is activated based on its predetermined schedule, it becomes the ion or electron that diffuses in the specified direction. When ions or electrons hit workpiece species, kinetic energy is transferred and gas molecules of workpiece species are generated. Chemical reaction and electron transfer can also be involved. For instance, the secondary ions of workpiece species and electrons can be generated.

Table 3 lists some examples of FIB lithography processes, assuming gallium ion is applied. R1 is the controlled event where gallium ions Ga^+ are generated according to the predetermined schedule. The locations of the controlled species Ga_src are also predetermined based on the milling path. R2 is the controlled trajectory of ions. R3–R6 are desorption paths of vaporized

Table 3 Example events in FIB lithography processes

Number of sites involved	Reaction/transition event
1	R1: Ga_src $\to$ Ga^+ (controlled)
2	R2: Ga^+ + vacancy $\to$ vacancy + Ga^+ (controlled) R3: workpiece_species_gas + vacancy $\to$ vacancy + workpiece_species_gas R4: workpiece_species$^+$ + vacancy $\to$ vacancy + workpiece_species$^+$ R5: Ga_gas + vacancy $\to$ vacancy + Ga_gas R6: e^- + vacancy $\to$ vacancy + e^- R7: workpiece_species_gas + absorbent $\to$ vacancy + absorbent R8: Ga_gas + absorbent $\to$ vacancy + absorbent R9: workpiece_species$^+$ + absorbent $\to$ vacancy + absorbent R10: e^- + absorbent $\to$ vacancy + absorbent
3	R11: Ga^+ + workpiece_species + vacancy $\to$ Ga_gas + vacancy + workpiece_species_gas R12: Ga^+ + workpiece_species + vacancy $\to$ Ga_gas + e^- + workpiece_species$^+$

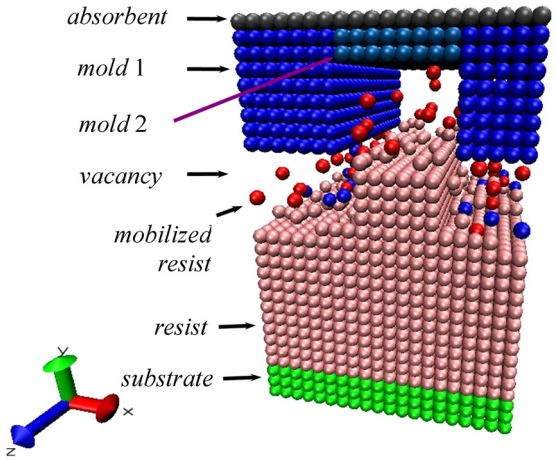

Fig. 3 Illustration of NIL events

workpiece species, secondary ions of workpiece species, neutralized gallium, and electrons, respectively. If the directions of paths are known, they can be controlled events too. R7–R10 define the simulation boundary. R11–R12 are examples of interaction between gallium ions and workpiece.

3.4.2 Nanoimprint Lithography (NIL). NIL is a promising approach to achieve high-precision high-throughput nanoscale patterning. Figure 3 illustrates the cKMC simulation of NIL. The mold may be represented by several controlled species at different locations. In the example shown in Fig. 3, the mold moves in the y direction. Equivalently in the implemented model, the controlled species are converted to vacancies gradually from bottom to top based on the specified speed. The interaction between the mold and the resist mobilizes the resist particles, which results in the situation that the geometry of pattern is not perfectly printed.

Table 4 shows some example events in the NIL process. R1 and R2 are controlled events where the controlled species are converted to vacancies in a controlled and deterministic manner. R3 characterizes the diffusion of mobilized resist species. R4 defines the boundary of simulated domains. R5 and R6 capture the interaction between the mold and the resist, where resist species may be mobilized. R7 is the adsorption process where mobilized resist species settle down.

In summary, it has been shown in this section how the proposed cKMC mechanism can be used to simulate top–down processes. Scanning probe lithography, FIB, and NIL are used to illustrate the mechanism. For soft lithography, it is similar to the nanoimprint lithography except that the detailed events and reaction rates need to be fine-tuned to reflect the specific processes. For photosynthesis type of processes, it is similar to the NIL where photons replace ions. Local self-assembly and chemical reactions can be easily incorporated as either self-assembly or controlled events.

Bottom-up processes can also be simulated by the cKMC simulation. In traditional KMC, bottom–up processes are simulated based on self-assembly events. Controlled events are useful in simulating some of the bottom–up processes, where traditional KMC is not capable of. For instance, in ultraviolet (UV) ablation of polymethylmethacrylate (PMMA) [43], radical photochemical reactions cause bond-breaks with new species generated, explosion of volumes, and particles ejected. In these cases, controlled events are reactions at selected locations. At a lower UV energy level, photothermal effects will cause melting and evaporation. Controlled events in this case are thermal diffusions. In ionized PVD, plasma particles only move within a confined space subject to electromagnetic fields to ionize vaporized metals. Ionized inert gas molecules such as argon travel and hit target metals under the guidance of electrical fields. These are also controlled events. In the following Sec. 3.4.3, ionized PVD is used to show how cKMC can simulate complete bottom–up processes.

3.4.3 Ionized PVD. Ionized PVD is an extension of the PVD technology that can achieve directional deposition of metals on substrates with high-aspect ratio features, such as vias and trenches. In the traditional PVD, it is difficult to let metal vapor travel deep enough into the bottom of vias. In ionized PVD, the sputtered or evaporated metal atoms go through the plasma sheath above substrate and ionized. External electrical field then guide ionized metal gas that can travel toward the bottom of vias.

The cKMC simulation of ionized PVD is shown in Fig. 4. There are an electron source and an argon gas source that inject electrons and argon gas into the domain. The plasma is generated and confined between the target and the substrate. Some examples of events are listed in Table 5. R1 and R2 are injection of argon gas and electrons. R3 to R5 are diffusions of argon (Ar), argon at the excited state (Ar*), and ionized argon (Ar^+), respectively. Ar* is generated by collision between electron and argon as in R10, and Ar^+ is generated by collision between electron and Ar* as in R11. Similarly, R6 to R8 are diffusions of metal (M), metal at the excited state (M*), and ionized metal (M^+), respectively. M* is generated by collision between electron and metal as in R12, and M^+ is generated by collision between electron and M* as in R13. Particularly, the diffusions of ionized argon (R5) and ionized metal (R8) are controlled events where the directions are controllable. R10 to R13 are also controlled where the collisions with electrons are toward the confined space of plasma sheath. R14 and R15 are adsorption events. Among events where three sites are involved, R16 and R17 are one-step ionization, where ionized argon and metal are generated from argon and metal directly without intermediate excited states. R18 is the metal ionization by collision with argon at the excited state. R19 is the bombardment of the target by ionized argon gas and metal atoms are sputtered out of the target. R20 to R23 are also adsorption events.

4 Implementation and Demonstration

4.1 Implementation. The proposed cKMC is implemented in C++ and integrated with SPPARKS [44], which is an open-source KMC toolbox developed at the Sandia National Laboratories.

Table 4 Example events in nanoimprint lithography processes

Number of sites involved	Reaction/transition event
1	R1: mold1 → vacancy (controlled) R2: mold2 → vacancy (controlled)
2	R3: mobilized_resist + vacancy → vacancy + mobilized_resist R4: mobilized_resist + absorbent → vacancy + absorbent
3	R5: mold1 + vacancy + resist → mold1 + mobilized_resist + vacancy R6: mold2 + vacancy + resist → mold2 + mobilized_resist + vacancy R7: mobilized_resist + resist + resist → resist + resist + resist

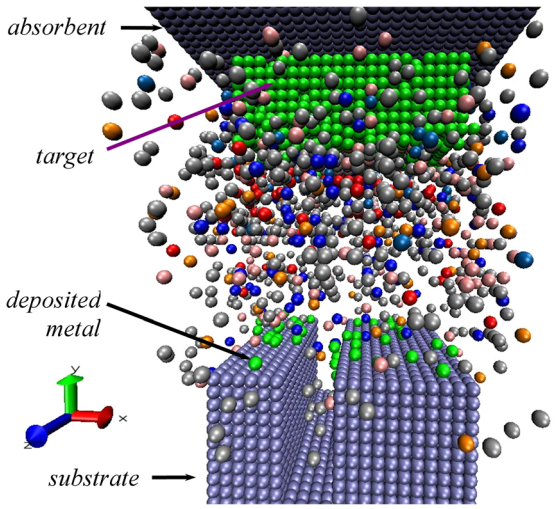

Fig. 4 Illustration of ionized PVD events

4.2 Demonstration. To demonstrate the effectiveness of the cKMC simulation, two examples of NIL are used. Figure 5(*a*) shows a scanning electron microscopy (SEM) image of a PMMA strip imprinted by a silicon dioxide mold [45]. The width of strips is about 70 nm. Figure 5(*b*) shows the result of cKMC simulation. A total of 590,400 sites are made in the model. One half of the sites are face centered cubic (fcc), and the other half are octahedral interstitial (octa). Each fcc site has 12 fcc and 6 octa neighbors, and each octa site has 6 fcc and 12 octa neighbors. The fcc sites are for the locations of regular particles, whereas the octa sites are for the particles with high kinetic energy and faster diffusion. Each particle has a diameter of 7 nm.

Compared to other top–down processes, NIL is more complex. Therefore it is chosen to demonstrate the sophistication that cKMC can achieve. When the deformation of resist is not significant as in scanning probe lithography and FIB, some of the controlled events for kinetic energy and mass transfer can be omitted in simulation, and the model can be further simplified.

The species and events used in the simulation are listed in Table 6. Figure 5(*c*) shows the different species in the simulation. Before the simulation starts, controlled species *path*1 defines the top–down traveling paths for the arrays of columns, whereas controlled species *path*2 defines the paths for the top portion of the mold. As simulation starts, *path*1 converts to *path*1_*active* at a preset speed specified by R1, similarly for *path*2 specified by R2, as the mold moves down. R3 and R4 model the upward movement of mold after it reaches the target position in press. Events of R3 and R4 start when the simulation clock reaches a preset time. Species *path*1_*active* is used to model the kinetic energy transfer between columns and resist while the mold is being pressed down, as shown R5. The fcc and octa indicate the sites where the reactants and products reside. As the mold moves down in R5, the column of mold presses resist toward sides and *mobilized_resist* at an octa site is created, which has high kinetic energy. R8 and R11 model the resist particles being dislocated to vacant space, and at the same time, *path*1_*active* is converted to *mold*1 that will be used in the upward movement of the mold later. These events mainly occur at the boundary of column where *vacancy* is available. For the inner portion of the column, the controlled event R5 models kinetic energy. The direction of the event diverges away from the center of the column. The mass transport is modeled as diffusion of *mobilized_resist* with high kinetic energy through octa sites as in R8.

R6 is a controlled event for the settling of *mobilized_resist* with the downward direction because of gravity. R7 defines the boundary of simulation domain. R9 and R10 model the repulsive interaction between the mold and resist. R12 captures the kinetic energy transfer from high-energy *mobilized_resist* to low-energy *mobilized_resist*. R13 is the diffusion of *mobilized_resist* with low kinetic energy, and R14 models the coordinated diffusion between two particles. R15 and R16 model the attractive interaction between the mold and resist. Finally R17 captures the cluster formation of resist. Notice that these 17 events are by no means exhaustive. More events can be identified and included to make the model more realistic at the cost of simulation time. A total of 7,160,284 events were fired within 11,340 central processing unit (CPU) seconds s or 3.15 hrs on a single-processor computer.

Table 5 Example events in ionized PVD processes

Number of sites involved	Reaction/transition event
2	R1: Ar_src + vacancy → Ar_src + Ar
	R2: e_src + vacancy → e_src + e^-
	R3: Ar + vacancy → vacancy + Ar
	R4: Ar* + vacancy → vacancy + Ar*
	R5: Ar^+ + vacancy → vacancy + Ar^+ (controlled)
	R6: M + vacancy → vacancy + M
	R7: M* + vacancy → vacancy + M*
	R8: M^+ + vacancy → vacancy + M^+ (controlled)
	R9: e^- + vacancy → vacancy + e^-
	R10: e^- + Ar → Ar* + e^- (controlled)
	R11: e^- + Ar* → Ar^+ + e^- (controlled)
	R12: e^- + M → M* + e^- (controlled)
	R13: e^- + M* → M^+ + e^- (controlled)
	R14: M + substrate → target + substrate
	R15: M + target → target + target
3	R16: e^- + Ar + vacancy→ Ar^+ + e^- + e^-
	R17: e^- + M + vacancy→ M^+ + e^- + e^-
	R18: Ar* + M + vacancy→ M^+ + Ar + e^-
	R19: Ar^+ + target + vacancy→ e^- + Ar + M
	R20: M + substrate + substrate → target + substrate + substrate
	R21: M^+ + substrate + substrate → target + substrate + substrate
	R22: M^+ + substrate + target → target + substrate + target
	R23: M^+ + target + target → target + target + target

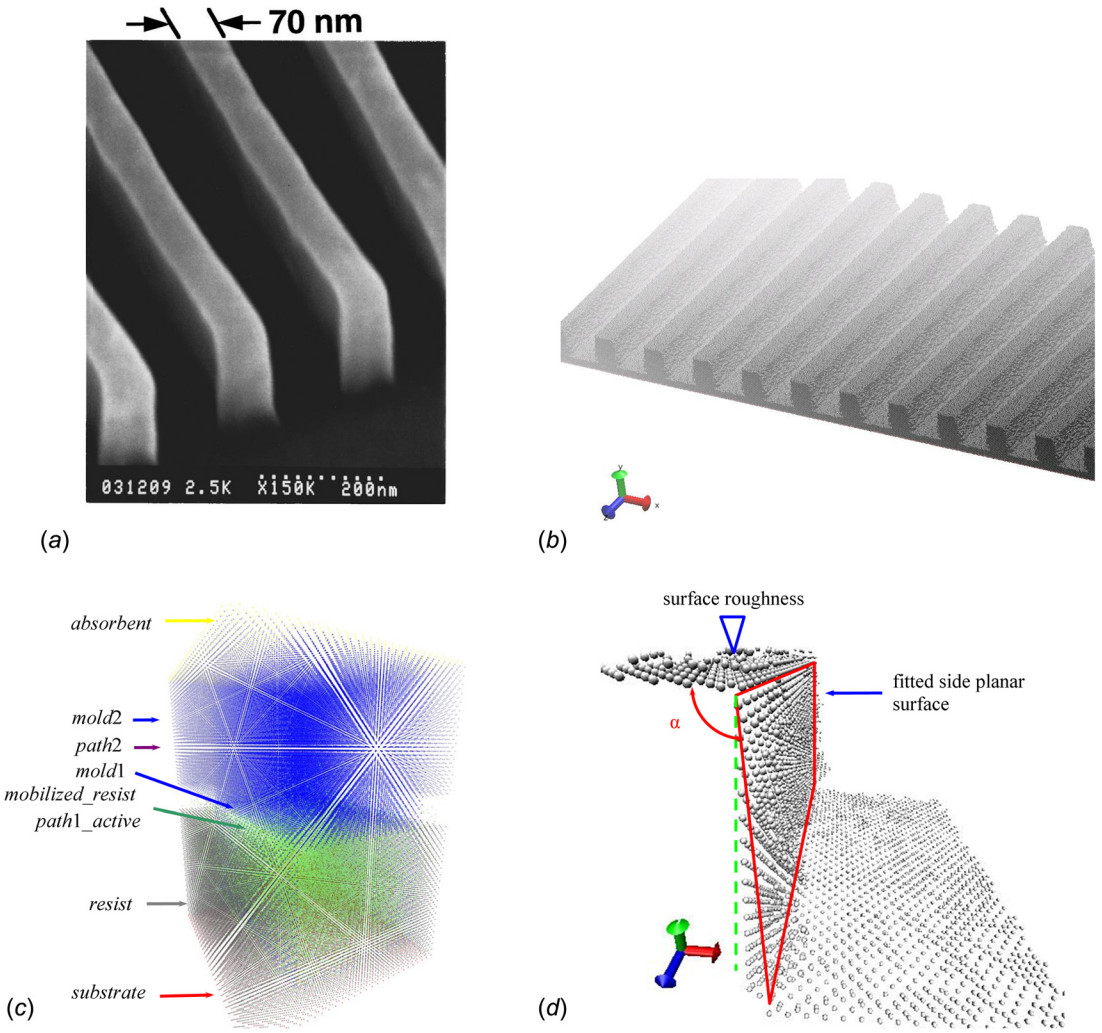

Fig. 5 cKMC model of NIL and the comparison between simulation and the SEM image from an experiment of a PMMA layer imprinted by a silicon dioxide mold. (*a*) SEM image of PMMA imprinted by silicon dioxide mold [45] (courtesy of Chou). (*b*) cKMC model of NIL process. (*c*) Species in NIL. (*d*) Surface roughness and angle estimated with particle coordinates from simulation result.

Table 6 Events of the cKMC model in Fig. 5

Number of sites involved	Reaction/transition event	Rate	Number of events
1	R1: path1 → path1_active (controlled)		35,520
	R2: path2 → mold2 (controlled)		22,080
	R3: mold1 → vacancy (controlled)		42,637
	R4: mold2 → vacancy (controlled)		22,080
2	R5: (fcc) path1_active + (octa) vacancy → vacancy + mobilized_resist (controlled)	1e −12	32,314
	R6: (fcc) mobilized_resist + (fcc) vacancy → vacancy + mobilized_resist (controlled)	1.0	28,176
	R7: (fcc) mobilized_resist + (fcc) absorbent → vacancy + absorbent	1e −12	2
	R8: (octa) mobilized_resist + (octa) vacancy → vacancy + mobilized_resist	1e −2	5,511,890
	R9: (fcc) mold1 + (fcc) resist → mold1 + mobilized_resist	1e −1	5243
	R10: (fcc) mold2 + (fcc) resist → mold2 + mobilized_resist	1e −1	0
3	R11: (fcc) path1_active + (octa) vacancy + (fcc) resist → mold1 + mobilized_resist + mobilized_resist	1e−12	3192
	R12: (octa) mobilized_resist + (fcc) mobilized_resist + (fcc) vacancy → vacancy + mobilized_resist + mobilized_resist	1e2	18
	R13: (fcc) mobilized_resist + (fcc) vacancy + (fcc) vacancy → vacancy + mobilized_resist + vacancy	5.0	1,286,661
	R14: (fcc) mobilized_resist + (fcc) mobilized_resist + (fcc) vacancy → mobilized_resist + vacancy + mobilized_resist	0.8	117,682
	R15: (fcc) mold1 + (fcc) vacancy + (fcc) resist → mold1 + mobilized_resist + vacancy	1e−1	22,245
	R16: (fcc) mold2 + (fcc) vacancy + (fcc) resist → mold2 + mobilized_resist + vacancy	1e−1	0
	R17: (fcc) mobilized_resist + (fcc) resist + (fcc) resist → resist + resist + resist	1.0	30,544

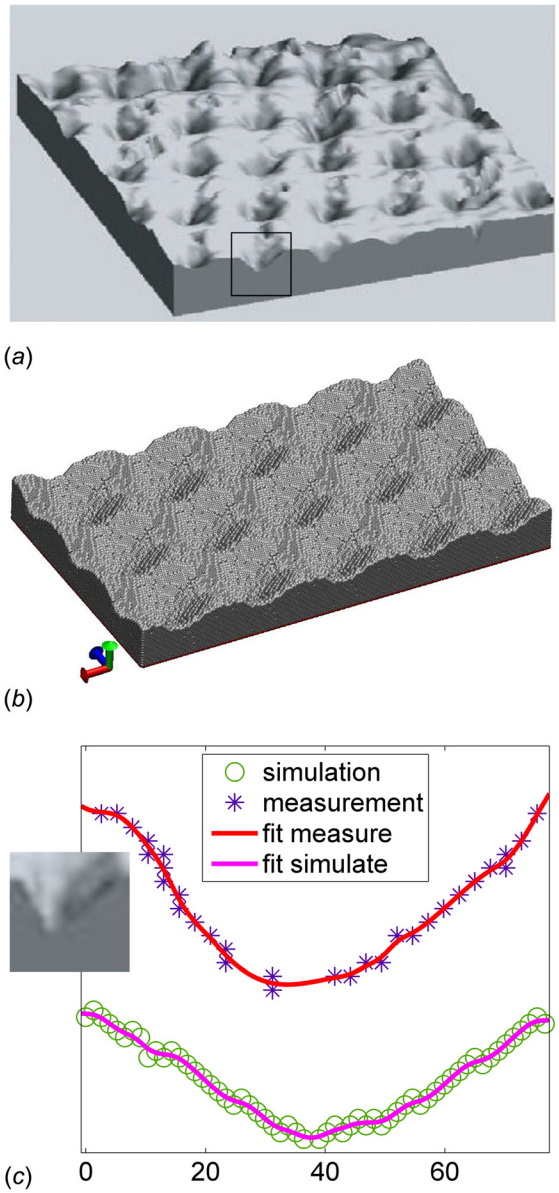

Fig. 6 cKMC model of NIL and the comparison between simulation and the SEM image from an experiment of a PMMA layer imprinted by a Cr stamp. (*a*) SEM image of PMMA imprinted by a Cr stamp [46] (courtesy of Sotomayor Torres). (*b*) cKMC simulation result. (*c*) comparison of the pattern profile between simulation and measurement.

Surface roughness and surface angles are used to compare the simulation result with the experiment. The reported roughness of the top surface in the experiment is about 3 nm [45]. As shown in Fig. 5(*d*), the roughness of the top surface in simulation is measured by the differences of Y coordinates of the 461 particles' on the top surface. The maximum difference between the Y coordinates is 7 nm. The root mean square of the differences between the coordinates and the average is 3.5 nm. The angle between the top and side surfaces is also compared. As shown in Fig. 5(*d*), 2007 particles are extracted as the side surface. The x, y, and z coordinates of the centers of these particles are taken to construct a planar surface with least-square-error fitting. The angle α between the fitted side plane and the top plane is calculated as 92.32 deg. The measured angle is reported to be about 90 deg [45].

As a second example, Fig. 6(*a*) shows a SEM image of a PMMA layer imprinted by a Chromium (Cr) stamp with an array of columns [46]. The columns have diameters of 50 nm and heights of 60 nm. The array of columns has a 100 nm period. Figure 6(*b*) shows the constructed cKMC model, which consists of 223,200 fcc sites and 223,200 octa sites. Figure 6(*b*) shows the simulation result when the simulation stops and the mold moves upward back to a specific position. Compared to the previous cKMC model of NIL, the geometry of this model is different. Different rate values for events were chosen to model different kinetics and material properties. For instance, the rates for R6, R8, R12, R13, R14, R15, and R17 are 0.001, 0.001, 1.0, 1.0, 5.0, 0.01, and 10.0, respectively in the second model. Additional events for coordinated diffusion of high-energy particles and energy transfer were also introduced, as listed in Table 7. In the simulation, the total time used to fire a total of 3,032,195 events is 5962 CPU seconds or 1.66 hrs on a single-processor computer. Note that the simulation time is directly proportional to the number of events fired instead of real wall time in physical processes. The cKMC can also be parallelized and run on multiprocessor computers to reduce simulation times.

The generated pattern profile from simulation is compared with one from the SEM image, as shown in Fig. 6(*c*). The edge of the profile in the SEM image is detected by applying the Prewitt filter. The continuous profile is fitted from the discrete pixel positions by the so-called smoothing spline method with the combination of the least-square error regression and a smoothness criterion. The profile of the simulation is first extracted as discrete positions of particles, then the smoothing spline method is also applied.

5 Concluding Remarks

In this paper, a generalized KMC mechanism, called controlled KMC, is introduced to simulate both top–down and bottom–up nanomanufacturing processes. A new concept of controlled event is introduced into the new cKMC mechanism so that events occurring at particular times, locations, or directions can be specified. Controlled event provides the mechanism of coupling deterministic processes with stochastic ones. Together with the traditional self-assembly events, controlled events can simulate complete physical and chemical processes. The cKMC mechanism is implemented and demonstrated by lattice-based examples of scanning probe lithography, FIB, NIL, and ionized PVD.

It should be emphasized that the purpose of the examples given in the paper is to demonstrate the feasibility of the new simulation mechanism for different processes. To accurately simulate a particular process, domain knowledge of the process is required to calibrate the input parameters and validate simulation models by comparing simulation outputs such as geometry accuracy, surface quality, and processing time with experimental results before they can be applied for prediction. Simulation specialists need to work with domain experts for specific processes. The most important factor to accurately simulate various nanomanufacturing processes with the generic cKMC mechanism is to find simulation

Table 7 Additional events of the cKMC model in Fig. 6

Reaction/transition event	Rate
(octa) mobilized_resist + (fcc) resist + (octa) vacancy → vacancy + mobilized_resist + mobilized_resist	1.0
(fcc) mobilized_resist + (fcc) mobilized_resist + (fcc) resist → mobilized_resist + mobilized_resist + mobilized_resist	1.0
(fcc) mobilized_resist + (fcc) mobilized_resist + (fcc) resist → resist + resist + resist	5.0

parameters, including a complete list of all possible events and the associated propensities or rates; this is the main limitation of KMC. This identification process usually requires full understanding the physical processes. If there is a lack of full understanding, first-principles simulation approaches may be applied to gain such insights.

The inputs of KMC models include events and rates. Reaction or transition events and the associated rates can be found and calibrated by either physical experiments empirically or first-principles simulation. Rather than the absolute values of rates, it is the relative differences among the rates that affect the simulation results because the selection of events in the KMC mechanism is based on the relative differences. For controlled events, the selection is further constrained by the time, location, or direction according to the accept–rejection scheme.

Sensitivity analysis is necessary for accurate cKMC simulation of a specific nanomanufacturing process. The sensitivity of simulation prediction with respect to the variation of inputs requires extensive computational experiments. In this study, it is found that simulation results are sensitively dependent on the rates of both controlled and self-assembly events. If necessary, extremely small or large rates can be chosen to ensure that events are fired immediately or nearly never will be fired.

References

[1] Lyons, K. W., 2007, "Integration, Interoperability, and Information Management: What are the Key Issues for Nanomanufacturing?," Proc. SPIE, **6648**, p. 66480D.

[2] Xia, Y., Rogers, J. A., Paul, K. E., and Whitesides, G. M., 1999, "Unconventional Methods for Fabricating and Patterning Nanostructures," Chem. Rev, **99**(7), pp. 1823–1848.

[3] Busnaina, A., ed., 2006, *Nanomanufacturing Handbook*, CRC Press, Boca Raton.

[4] Tseng, A. A., ed., 2008, *Nanofabrication: Fundamentals and Applications*, World Scientific Publishing, Singapore.

[5] Komanduri, R., and Raff, L. M., 2001, "A Review on the Molecular Dynamics Simulation of Machining at the Atomic Scale," Proc. Inst. Mech. Eng., Part B, **215**(12), pp. 1639–1672.

[6] Fang, T.-H., Weng, C.-I., and Chang, J.-G., 2002, "Molecular Dynamics Simulation of Nano-Lithography Process Using Atomic Force Microscopy," Surf. Sci., **501**(1), pp. 138–147.

[7] Jun, S., Lee, Y., Kim, S. Y., and Im, S., 2004, "Large-Scale Molecular Dynamics Simulations of Al(111) Nanoscratching," Nanotechnology, **15**(9), pp. 1169–1174.

[8] Komanduri, R., Chandrasekaran, N., and Raff, L. M., 1998, "Effect of Tool Geometry in Nanometric Cutting: A Molecular Dynamics Simulation Approach," Wear, **219**(1), pp. 84–97.

[9] Komanduri, R., Chandrasekaran, N., and Raff, L. M., 2001, "Molecular Dynamics Simulation of the Nanometric Cutting of Silicon," Philos. Mag. B, **81**(12), pp. 1989–2019.

[10] Yang, Y., Chen, S., Cheng, K., and Sun, X., 2007, "Diamond Turning of Microstructured Surfaces: Modeling and Simulation," Int. J. Nanomanuf., **1**(5), pp. 627–640.

[11] Han, X., 2007, "Study Micromechanism of Surface Planarization in the Polishing Technology Using Numerical Simulation Method," Appl. Surf. Sci., **253**(14), pp. 6211–6216.

[12] Shimada, S., Ikawa, N., Inamura, T., Takezawa, N., Ohmori, H., and Sata, T., 1995, "Brittle-Ductile Transition Phenomena in Microindentation and Micromachining," CIRP Ann. Manuf. Technol., **44**(1), pp. 523–526.

[13] Stavropoulos, P., and Chryssolouris, G., 2007, "Molecular Dynamics Simulations of Laser Ablation: The Morse Potential Function Approach," Int. J. Nanomanuf., **1**(6), pp. 736–750.

[14] Wang, N., Rokhlin, S. I., and Farson, D. F., 2007, "Nanoparticle Coalescence and Sintering: Molecular Dynamics Simulation," Int. J. Nanomanuf., **1**(6), pp. 810–824.

[15] Voter, A. F., 1998, "Parallel Replica Method for Dynamics of Infrequent Events," Phys. Rev. B, **57**(22), pp. R13985–R13988.

[16] Voter, A. F., 1997, "Hyperdynamics: Accelerated Molecular Dynamics of Infrequent Events," Phys. Rev. Lett., **78**(20), pp. 3908–3911.

[17] Sørensen, M. R., and Voter, A. F., 2000, "Temperature-Accelerated Dynamics for Simulation of Infrequent Events," J. Chem. Phys., **112**(21), pp. 9599–9606.

[18] Chatterjee, A., and Vlachos, D. G., 2007, "An Overview of Spatial Microscopic and Accelerated Kinetic Monte Carlo Methods," J. Comp. Aided Mat. Des., **14**(2), pp. 253–308.

[19] Lasrado, V., Alhat, D., and Wang, Y., 2008, "A Review of Recent Phase Transition Simulation Methods: Transition Path Search," ASME Paper No. DETC2008-49410.

[20] Alhat, D., Lasrado, V., and Wang, Y., 2008, "A Review of Recent Phase Transition Simulation Methods: Saddle Point Search," ASME Paper No. DETC2008-49411.

[21] Gillespie, D. T., 1976, "A General Method for Numerically Simulating the Stochastic Evolution of Coupled Chemical Reactions," J. Comput. Phys., **22**(4), pp. 403–434.

[22] Maksym, P. A., 1988, "Fast Monte Carlo Simulation of MBE Growth," Semicond. Sci. Technol., **3**(6), pp. 594–596.

[23] Blue, J. L., Beichl, I., and Sullivan, F., 1995, "Faster Monte Carlo Simulations," Phys. Rev. E, **51**(2), pp. R867–R868.

[24] Schulze, T. P., 2008, "Efficient Kinetic Monte Carlo Simulation," J. Comput. Phys., **227**(4), pp. 2455–2462.

[25] Wang, Y., 2013, "Reliable Kinetic Monte Carlo Simulation Based on Random Set Sampling," Soft Comput., **17**(8), pp. 1439–1451.

[26] Yang, Y. G., Johnson, R. A., and Wadley, H. N. G., 1997, "A Monte Carlo Simulation of the Physical Vapor Deposition of Nickel," Acta Mater., **45**(4), pp. 1455–1468.

[27] Huang, H., Gilmer, G. H., and Diaz de la Rubia, T., 1998, "An Atomistic Simulator for Thin Film Deposition in Three Dimensions," J. Appl. Phys., **84**(7), pp. 3636–3649.

[28] Yang, Y. G., Zhou, X. W., Johnson, R. A., and Wadley, H. N. G., 2001, "Monte Carlo Simulation of Hyperthermal Physical Vapor Deposition," Acta Mat., **49**(16), pp. 3321–3332.

[29] Wang, L., and Clancy, P., 2001, "Kinetic Monte Carlo Simulation of the Growth of Polycrystalline Cu Films," Surf. Sci., **473**(1–2), pp. 25–38.

[30] Dalla Torre, J., Bilmer, G. H., Windt, D. L., Kalyanaraman, R., Baumann, F. H., O'Sullivan, P. L., Sapjeta, J., Diaz de la Rubia, T., and Djafari Rouhani, M., 2003, "Microstructure of Thin Tantalum Films Sputtered Onto Inclined Substrates: Experiments and Atomistic Simulations," J. Appl. Phys., **94**(1), pp. 263–271.

[31] Battaile, C. C., Srolovitz, D. J., and Butler, J. E., 1997, "A Kinetic Monte Carlo Method for the Atomic-Scale Simulation of Chemical Vapor Deposition: Application to Diamond," J. Appl. Phys., **82**(12), pp. 6293–6300.

[32] Battaile, C. C., and Srolovitz, D. J., 2002, "Kinetic Monte Carlo Simulation of Chemical Vapor Deposition," Annu. Rev. Mater. Res., **32**(1), pp. 297–319.

[33] Grujicic, M., and Lai, S. G., 1999, "Atomistic Simulation of Chemical Vapor Deposition of (111)-Oriented Diamond Film Using a Kinetic Monte Carlo Method," J. Mater. Sci., **34**(1), pp. 7–20.

[34] Kalke, M., and Baxter, D. V., 2001, "A Kinetic Monte Carlo Simulation of Chemical Vapor Deposition: Non-Monotonic Variation of Surface Roughness With Growth Temperature," Surf. Sci., **477**(2), pp. 95–101.

[35] Flidr, J., Huang, Y.-C., Newton, T. A., and Hines, M. A., 1998, "Extracting Site-Specific Reaction Rates From Steady State Surface Morphologies: Kinetic Monte Carlo Simulations of Aqueous Si(111) Etching," J. Chem. Phys., **108**(13), pp. 5542–5553.

[36] Netto, A., and Frenklach, M., 2005, "Kinetic Monte Carlo Simulations of CVD Diamond Growth—Interlay Among Growth, Etching, and Migration," Diamond Relat. Mater., **14**(10), pp. 1630–1646.

[37] Zhou, H., Fu, J., and Silver, R. M., 2007, "Time-Resolved Kinematic Monte-Carlo Simulation Study on Si(111) Etching," J. Phys. Chem., **111**(9), pp. 3566–3574.

[38] Battaile, C. C., Srolovitz, D. J., Oleinik, I. I., Pettifor, D. G., Sutton, A. P., Harris, S. J., and Butler, J. E., 1999, "Etching Effects During the Chemical Vapor Deposition of (100) Diamond," J. Chem. Phys., **111**(9), pp. 4291–4299.

[39] Kratzer, P., and Scheffler, M., 2002, "Reaction-Limited Island Nucleation in Molecular Beam Epitaxy of Compound Semiconductors," Phys. Rev. Lett., **88**(3), p. 036102(1-4).

[40] Mei, D., Ge, Q., Neurock, M., Kieken, L., and Lerou, J., 2004, "First-Principles-Based Kinetic Monte Carlo Simulation of Nitric Oxide Decomposition Over Pt and Rh Surfaces Under Lean-Burn Conditions," Mole. Phys., **102**(4), pp. 361–369.

[41] Stumpf, R., and Scheffler, M., 1994, "Theory of Self-Diffusion at and Growth of Al(111)," Phys. Rev. Lett., **72**(2), pp. 254–257.

[42] Bogicevic, A., Hyldgaard, P., Wahnström, G., and Lundqvist, B. I., 1998, "Al Dimmer Dynamics on Al(111)," Phys. Rev. Lett., **81**(1), pp. 172–175.

[43] Prasad, M., Conforti, P. F., Garrison, B. J., and Yingling, Y. G., 2007, "Computational Investigation Into the Mechanisms of UV Ablation of Poly(methyl methacrylate)," Appl. Surf. Sci., **253**(15), pp. 6382–6385.

[44] Plimpton, S., Thompson, A., and Slepoy, A., SPPARKS Kinetic Monte Carlo Simulator. http://spparks.sandia.gov/

[45] Chou, S. Y., Krauss, P. R., and Renstrom, P. J., 1996, "Nanoimprint Lithography," J. Vac. Sci. Technol. B, **14**(6), pp. 4129–4133.

[46] Zankovych, S., Hoffmann, T., Seekamp, J., Bruch, J.-U., and Sotomayor Torres, C. M., 2001, "Nanoimprint Lightography: Challenges and Prospects," Nanotechnology, **12**(2), pp. 91–95.